Dual-band Transceiver with Mutually-coupled On-chip Antennas for Implantable/Wearable Devices

Nilan Udayanga and Manuel Monge
University of Southern California, Los Angeles, CA, 90089, USA
udayanga@usc.edu and manuel.monge@usc.edu

***Abstract*—This paper presents a fully integrated dual-band transceiver (TRX) with mutually-coupled on-chip antennas for implantable and wearable devices. It operates at 915 MHz and 2.4 GHz in both transmit and receive modes to enable bidirectional communication between medical and consumer electronics using a single chip. The TRX is fabricated in 180 nm CMOS along with a power management unit (PMU) with a size of 2.4×1.9 mm^2. The PMU generates the required supplies to power the internal TRX, external sensors, and controller units from a single battery. The transmitter (TX) consists of a mutually-coupled dual-band oscillator and uses the on-chip antennas as the inductors of the oscillators. The maximum uplink data rates of the TXs are 20 Mb/s and 40 Mb/s for 915 MHz and 2.4 GHz, respectively, with corresponding TX efficiencies of 62 pJ/b and 35 pJ/b. The maximum achievable downlink data rates are 2 Mb/s and 1 Mb/s for 915 MHz and 2.4 GHz, respectively, resulting in 2 pJ/b and 4 pJ/b of energy efficiencies. Importantly, the proposed TRX achieves uplink and downlink communication ranges of 30 cm and 17 cm for the 915 MHz band, and of 38 cm and 2 cm for the 2.4 GHz band, respectively.**

***Index Terms*—Dual-band transceiver, Mutually-coupled antennas, Implantable devices, Wearable devices.**

I. Introduction

Recent progress in implantable and wearable technologies has made them an important tool for physicians to monitor biophysical parameters, diagnose numerous health conditions, and treat diseases. Applications of such devices include drug delivery systems, neural interfaces, vital sign sensors, and intraocular pressure sensors [1]–[3]. Implantable and wearable devices demand low power consumption, small form factor (mm-scale), and wireless connectivity. In such devices, the transceiver (TRX) dominates the overall power (data transmission) and area (passive components and antenna) consumption. Thus, the main goal in designing implantable/wearable transceivers (IWTs) is to achieve a high data rate and communication range with less power and area. Current single-band IWTs achieve Mb/s of data rates and pJ/bit of energy efficiencies for cm-scale communication ranges [4]–[7].

Most medical devices currently operate at 400-430 MHz or at 900-915 MHz (due to less absorption by body tissues) whereas most consumer electronics such as mobile phones and smartwatches support 2.4 GHz. This mismatch between medical devices and consumer electronics hinders their natural communication ability and requires additional components to create a full system solution. The resulting sub-optimal system will be bigger, less efficient, and will limit otherwise possible biomedical applications. In addition, most of the existing IWTs have used off-chip antennas to improve the communication range by trading off the size of the complete system [4]–[6].

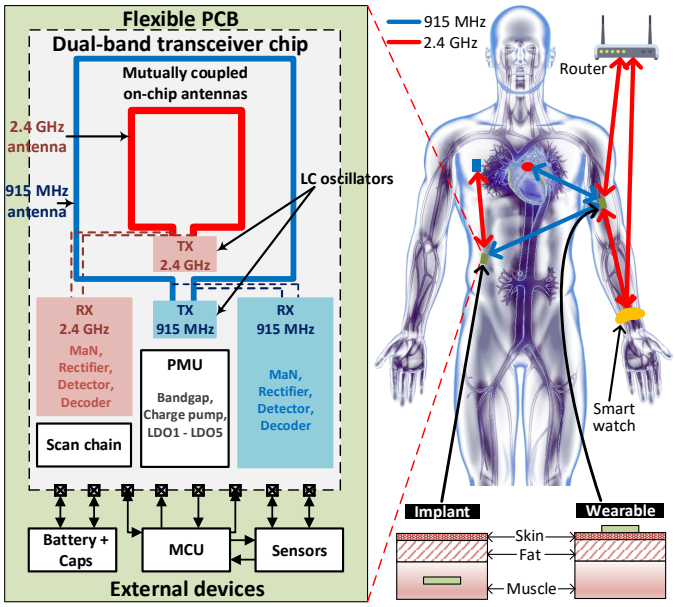

Fig. 1: Left: System architecture of the proposed dual-band TRX. Right: Intended applications of the TRX as an implant and wearable.

In this work, we present a 2.4 ×1.9 mm^2 dual-band IWT that addresses these limitations by operating at 915 MHz and 2.4 GHz in both transmit and receive modes, and achieving cm-range bidirectional communication using on-chip antennas. The proposed TRX provides a unique connecting platform between medical and consumer electronics in a single chip and enables a wide variety of applications including implantable and wearable devices, body area networks, and health monitoring systems. For IWTs, the data rate requirement for uplink (TRX to an external system) and downlink (external system to TRX) is usually asymmetric. Higher data rates are required for uplink (to support multi-channel sensor data as in neural recording) than downlink (only controlling and actuation signals) [1]. The proposed IWT uses this information to minimize its power and area consumption. It achieves up to 38 cm and 17 cm of communication distance, and maximum data rates up to 40 Mb/s and 2 Mb/s for the uplink and downlink, respectively, with less than 70 pJ/bit of energy efficiencies.

II. Mutually-coupled Dual-band Transceiver

Fig. 1 shows the block diagram of the proposed dual-band TRX with a power management unit (PMU). The CMOS

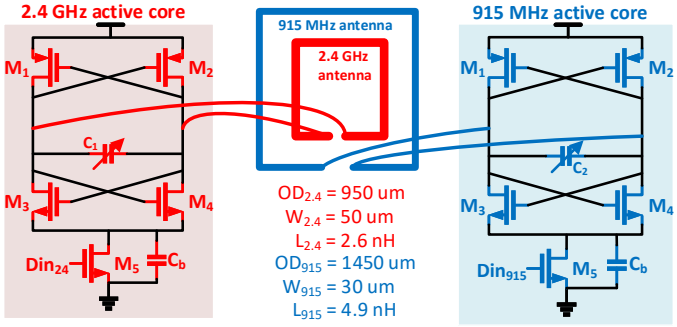

Fig. 2: Schematic of the dual-band dual-port LC oscillator with mutually-coupled inductors (antennas).

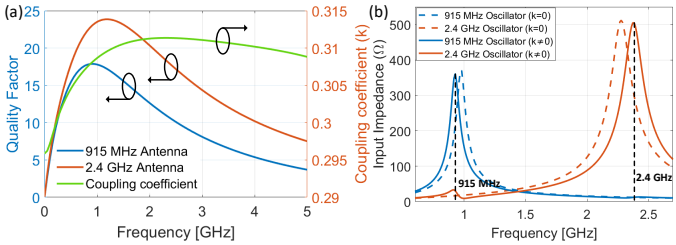

Fig. 3: (a) Variation of the quality factors of the individual loops when they are placed in a concentric configuration and the simulated coupling coefficient (k) of the designed mutually-coupled antennas. (b) The magnitude input impedance looking into the two ports with and without mutual coupling.

chip consists of two mutually-coupled antennas, a dual-band dual-port LC oscillator-based transmitter (TX), rectifier-based receivers (RXs), a PMU, and a scan chain. The fabricated chip will be interconnected on a flexible printed circuit board (PCB) with external sensors, capacitors, controller units, and a single battery to be used as an implantable/wearable medical device. The PMU generates the required supplies to power the internal TRX and external sensors, actuators, and controller units from a single battery. The TRX time multiplexes the antennas to transmit and receive data. In an intended application (see Fig. 1), external devices (medical devices or consumer electronics) can request data using either frequency band. Following the request, the chip-enabled device initiates the controlling signals to extract the sensing data from the external sensors. The extracted data can then directly modulate the TX to communicate with the external system. The TRX supports both on-off keying with pulse width modulation (OOK-PWM) and standard OOK modulation. Similarly, the dual-band TRX can operate as a relay (or a hub) in-between other medical devices and smart mobile devices, that only operate at either 915 MHz or 2.4 GHz frequency bands.

A. Mutually-coupled On-chip Antennas

Two on-chip rectangular loops have been custom designed as the antennas of the proposed TRX, and are also used as the inductors of the LC oscillators (Fig. 2). The two antennas are placed in a concentric configuration to reduce the chip area and are optimized to enhance the near-field coupling between them and the external system. Based on electromagnetic simulations through HFSS, the antennas exhibit 15-20 dB improved electric and magnetic fields at a distance of 5 cm away from the antenna, compared to a standard multi-turn inductor (outer diameter OD = 410 μm, 4 turns) with similar inductance. Fig. 2 shows the OD, width (W), and simulated inductances of the 915 MHz and 2.4 GHz antennas. Fig. 3(a) shows the variation of the quality factors of the individual loops in a concentric configuration, with both antennas exhibiting a quality factor (Q) $\sim$18 at their resonance frequencies.

B. Transmitter: Dual-band Dual-port Oscillator

The proposed TX (Fig. 2) directly feeds the oscillator signals to the antennas without using a separate power amplifier (PA), reducing both the power consumption and chip area compared to a PA+oscillator architecture. A fourth-order, dual-port resonator with separate LC tanks has been designed, where the two inductors (antennas) are placed in a concentric configuration. Their coupling coefficient (k) was kept at less than 0.4 to sustain steady-state oscillation at both frequency bands [8], with a simulated value of $\sim$0.3 throughout the required frequency range (Fig. 3(a)). The geometry of the 2.4 GHz antenna is selected such that the impedance looking into its input port shows a higher peak than that of the 915 MHz antenna when k=0. This asymmetry allows having a sufficient peak at both frequencies when the two inductors are mutually coupled, even if k increases due to the changes in the surrounding environment (Fig. 3(b)). Capacitors C_1 and C_2 are realized using 3-bit capacitor arrays to compensate for PVT variations. The active core of the dual-band oscillator is designed using CMOS cross-coupled pairs powered by 1.2 V.

C. Receiver: Fully-differential Full-wave Rectifier

The receiver consists of a dual RX chain with a switch, a matching network, a rectifier, decoder 1 (DC_1), and decoder 2 (DC_2) per band (Fig. 4). A rectifier-based RX is selected because of its low power and area consumption compared to low noise amplifier (LNA)-based RX and the low data-rate requirements of IWTs. The passive gain of the matching network is important in the absence of an LNA to improve the sensitivity of the RX. The simulated passive gains of the 915 MHz and 2.4 GHz matching networks are 6.2 dB and 5.0 dB, respectively. The rectifier is a cascade of four cross-connected differential rectifiers. Low threshold voltage transistors are used to achieve a low turn-on voltage, which mainly determines the sensitivity of the RX. OOK data is recovered at DC_1 by comparing the rectified output with a dynamic reference generated by averaging this output using a low-pass filter. A Schmitt-trigger follows the comparator to decrease noise sensitivity. For OOK-PWM, the output of DC_1 is fed into DC_2 to be first integrated throughout the pulse width and then compared with a pre-defined threshold voltage. The comparator in DC_2 will output '1' or '0' based on the integrated pulse duration.

D. Power Management Unit

The chip is powered by a single 1.5 V battery. The PMU consists of a bandgap reference, five low-dropout (LDO) regulators (LDO1 to LDO5), a charge pump, and a relaxation oscillator. The RX and TX supplies are generated using LDO1 (1 V) and LDO2 (1.2 V), respectively. Internal digital circuitry

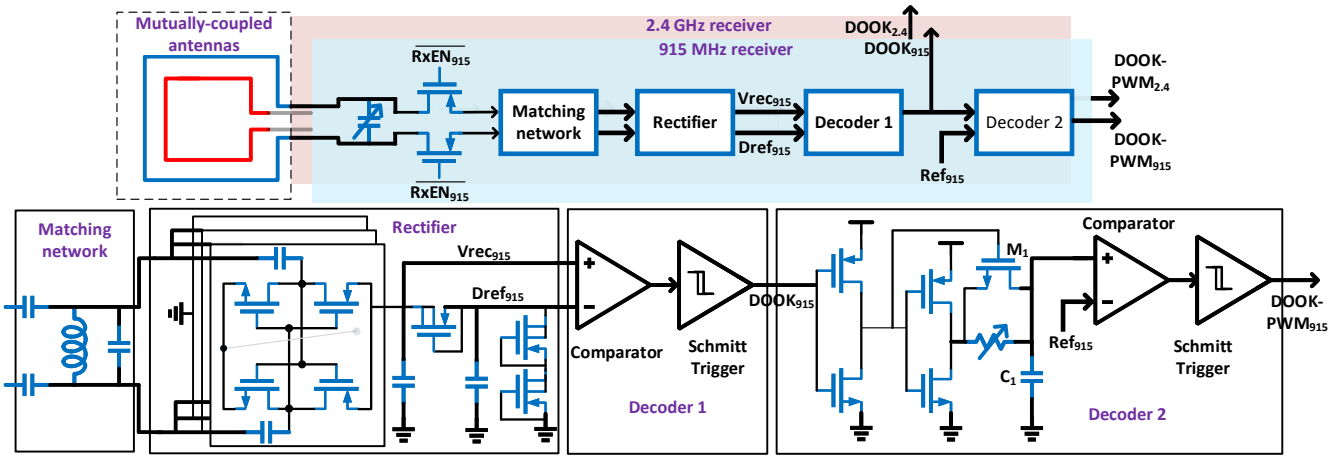

Fig. 4: Schematic of the dual-band receiver.

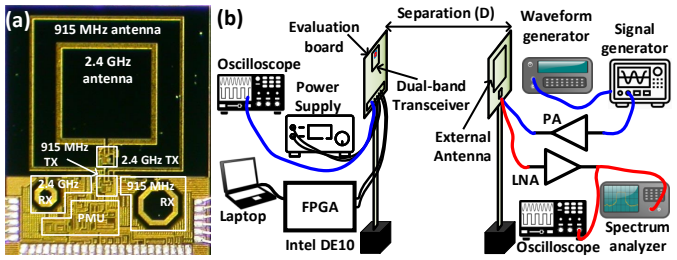

Fig. 5: (a) Chip micrograph. (b) Block-level diagram of the measurement setup for uplink (devices that connect using black and red cables) and downlink (devices that connect using black and blue cables) communications.

is powered by LDO3 (1.2 V). The external controller and sensors requiring a 1.8 V supply are powered using LDO4 and LDO5. The bandgap employs a pre-regulator to achieve a PSRR of -60 dB at 1 MHz. LDO1, LDO2, and LDO3 are stabilized using on-chip capacitors (100 pF), while LDO4 and LDO5 using external capacitors ($\sim$20 μF). A charge pump is used to double the 1.5 V battery voltage and provide the input for LDO4 and LDO5. The clock signals for the charge pump are generated using a current-mode relaxation oscillator.

III. Measurement Results

A prototype dual-band TRX has been fabricated in 180 nm CMOS (Fig. 5(a)). The block-level diagram of the measurement setup to test uplink (UL) and downlink (DL) is shown in Fig. 5(b). A 915 MHz loop antenna was utilized as the external antenna for the 915 MHz UL and DL measurements. For 2.4 GHz UL and DL, the external antenna was a wideband Vivaldi antenna and a 2.4 GHz loop antenna, respectively.

For the UL, the transmitted signals from the chip are first received at the external loop antenna, then amplified, and finally captured by an oscilloscope. This data is post-processed using MATLAB. Fig. 6(a) shows the post-processed received signal when the 915 MHz TX transmits a bitstream 01101001 (OOK) at 20 Mb/s with the external receiver place 30 cm away. The TX power consumption is 1.25 mW, which leads to an energy efficiency of 62 pJ/b. Fig. 6(b) shows the corresponding results for the 2.4 GHz TX, with an energy efficiency of 35 pJ/b at 40 Mb/s (communication distance is 38 cm).

For the DL, the outputs of the on-chip RXs are captured directly in the oscilloscope. Fig. 6(c) shows the decoded signal

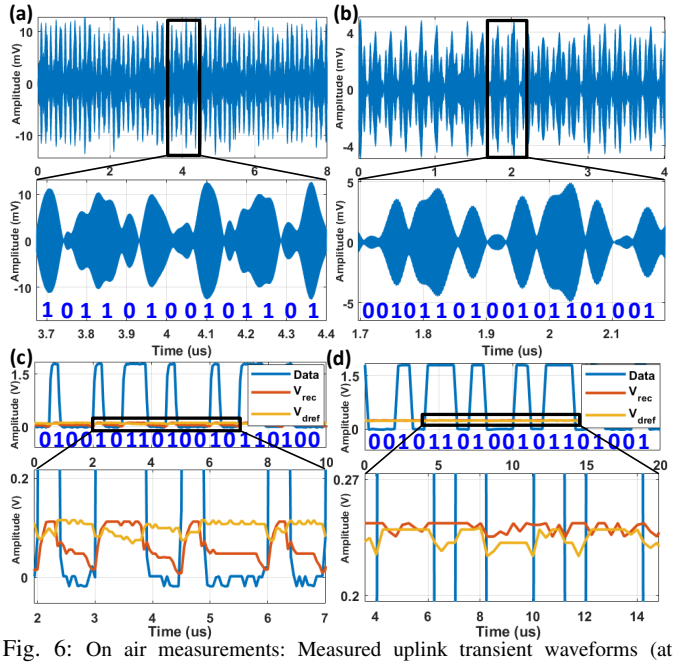

Fig. 6: On air measurements: Measured uplink transient waveforms (at the external antenna) of the (a) 915 MHz OOK and (b) 2.4 GHz OOK communications. Measured downlink transient waveforms (at the on-chip receiver) of the (c) 915 MHz OOK and (d) 2.4 GHz OOK communications.

for 915 MHz communication at 2 Mb/s where the distance between the two antennas is 11 cm. The figure also shows the variation of rectified output V_{rec} and dynamic reference D_{ref}. The power consumption of the 915 MHz RX is measured to be 4 μW resulting in 2 pJ/b energy efficiency. Fig. 6(d) shows the DL results for 2.4 GHz link (1 Mb/s, 1 cm distance, 4 μW of power consumption) with 4 pJ/b of energy efficiency. The 2.4 GHz downlink can also achieve 100 kbps at a 2 cm distance.

Fig. 7(a) shows the post-processed UL signal for OOK-

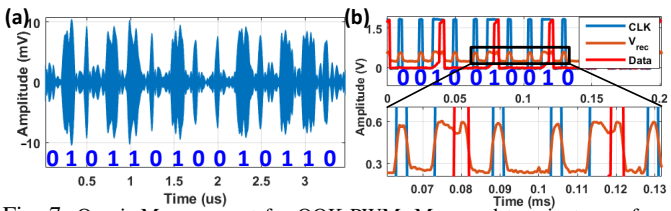

Fig. 7: On air Measurement for OOK-PWM: Measured transient waveform for (a) 2.4 GHz UL and (b) 915 MHz DL (clock CLK, V_{reg}, and Data).

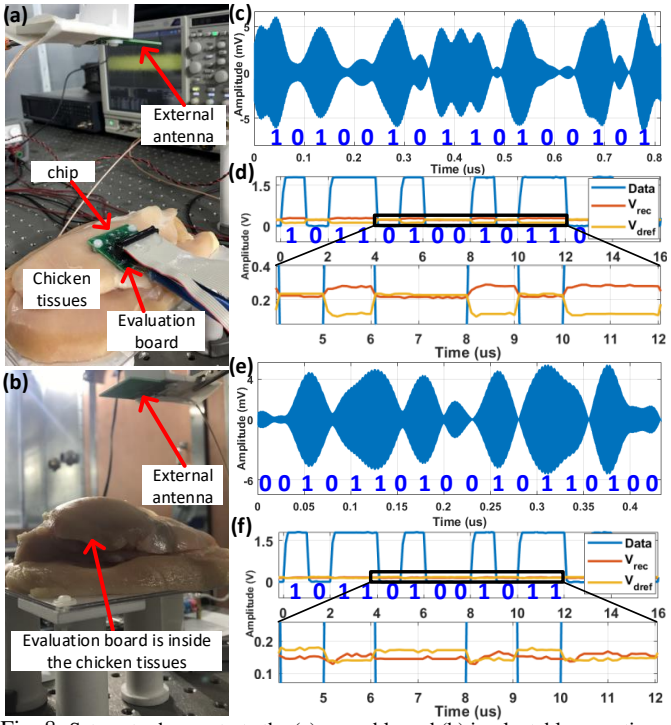

Fig. 8: Setups to demonstrate the (a) wearable and (b) implantable operations. Measurements as a wearable: (c) 2.4 GHz UL and (d) 915 MHz DL signals. Measurements as an implant: (e) 2.4 GHz UL and (f) 915 MHz DL signals.

TABLE I. COMPARISON WITH STATE OF THE ARTS

	This work		TCAS-II 2021 [4]	TBCAS 2020 [5]	CICC 2020 [7]	RFIC 2020 [6]
Technology [nm]	180		180	180	180	65
Single/dual-band	Dual		Single	Single	Single	Single
Powering method	Battery		Resonator	Battery	RF power	Battery
Antenna	On-chip		Off-chip	Off-chip	On-chip	Off-chip
Modulation TX	OOK/OOK-PWM		OOK/FSK	OOK	OOK/UWB	OOK
Modulation RX	OOK/OOK-PWM		-	OOK	ASK	-
TX Freq [MHz]	915	2400	2400	2400	4150	400.9
RX Freq [MHz]	915	2400	-	2400	250	-
TX Pwr [mW]	1.25 @20 Mb/s	1.4 @40 Mb/s	0.07	0.6	0. 698	0.05
RX Pwr [uW]	4	4	-	160	2.6	-
TX data rate [Mbps]	20 @ 30 cm	40 @ 38 cm	10	20	150	10
RX data rate [Mbps]	2 @ 11 cm	1 @ 1 cm	-	2	2.5	-
TX Effi [pJ/b]	62	35	7	30	4.65	4.93
RX Effi [pJ/b]	2	4	-	80	1	-
TX transmit power [dBm]	-6*	0*	-33	-17	N/A	-19.9
Maximum range [cm]	30 (UL)/ 13 (DL)	38 (UL)/ 2 (DL)	20	38	15 (UL)/ 1 (DL)	N/A
Die area [mm^2]	4.56		0.02	2.9	5.28	0.062

*Estimated

PWM modulation at 2.4 GHz (4 Mb/s, 28 cm distance, 1 mW of power, energy efficiency of 270 pJ/b). Fig. 7(b) shows the decoded data, V_{rec}, and clock (CLK, DOOK) signals for 915 MHz OOK-PWM modulated DL (75 kb/s, 9 cm distance).

The TRX has been fully tested emulating wearable and implantable operations (both bands, UL and DL). Fig. 8 shows only one case of each. To emulate wearable operation, the chip is placed on top of fresh animal tissue (Fig. 8(a)). Fig. 8(c) shows the 2.4 GHz UL signal (20 Mb/s, 14 cm on air). The 915 MHz DL signals are shown in Fig. 8 (d) (1 Mb/s, 3.5 cm on air). To demonstrate implantable operation, the chip is placed inside the animal tissue (Fig. 8(b)). Fig. 8(e) shows the 2.4 GHz UL signal at the external antenna (40 Mb/s, 6 cm on air, and 1 cm of tissue). The 915 MHz DL signals are shown in Fig. 8(f) (1 Mb/s, 2 cm on air, and 1 cm of tissue).

The proposed dual-band TRX is capable of simultaneous transmission and reception using both frequency bands. As an implantable TRX, the 915 MHz and 2.4 GHz TXs achieved 16 Mb/s and 20 Mb/s of data rates when both TXs operate simultaneously. The total power consumption is 2.35 mW. The on-air distances are 11 cm and 6 cm for 915 MHz and 2.4 GHz links, respectively, with the chip 1 cm underneath the chicken tissue. The resulting energy efficiency is 67 pJ/b. The simultaneous reception has been tested on air by placing the 915 MHz and 2.4 GHz antennas 7 cm and 0.75 cm away from the chip, respectively. The data rates of the 915 MHz and 2.4 GHz DLs are 100 b/s and 2 Kb/s, respectively. Table I compares the dual-band TRX with the state of the art.

IV. CONCLUSION

This work reports a dual-band TRX with mutually-coupled on-chip antennas for implantable and wearable devices in 180 nm CMOS. To the best of our knowledge, this is the first implementation of such TRX capable of bidirectional communication in implantable and wearable devices with simultaneous transmission (or reception) at both frequency bands. This is achieved by utilizing mutually-coupled on-chip antennas, LC oscillator-based TXs, and rectifier-based RXs. The fabricated prototype occupies an area of 2.4×1.9 mm^2 and achieves maximum data rates of 40 Mb/s for UL and 2 Mb/s for DL, up to 38 cm of range, and less than 70 pJ/b of energy efficiencies for different communication scenarios. The chip can be integrated with sensors on a flexible PCB to design a fully-wireless miniaturized implantable/wearable device.

REFERENCES

[1] S. A. Mirbozorgi, H. Bahrami, M. Sawan, L. A. Rusch, and B. Gosselin, "A single-chip full-duplex high speed transceiver for multi-site stimulating and recording neural implants," *IEEE Transactions on Biomedical Circuits and Systems*, vol. 10, no. 3, pp. 643–653, 2016.

[2] M. Konijnenburg *et al.*, "22.1 a 769w battery-powered single-chip SoC with BLE for multi-modal vital sign health patches," in *2019 IEEE Int. Solid- State Circuits Conference - (ISSCC)*, 2019, pp. 360–362.

[3] H. Bhamra *et al.*, "A subcubic millimeter wireless implantable intraocular pressure monitor microsystem," *IEEE Transactions on Biomedical Circuits and Systems*, vol. 11, no. 6, pp. 1204–1215, 2017.

[4] H. Bhamra, Y. W. Huang, Q. Yuan, and P. Irazoqui, "An ultra-low power 2.4 GHz transmitter for energy harvested wireless sensor nodes and biomedical devices," *IEEE Transactions on Circuits and Systems II: Express Briefs*, vol. 68, no. 1, pp. 206–210, 2021.

[5] S. Y. Lee, P. H. Cheng, C. F. Tsou, C. C. Lin, and G. S. Shieh, "A 2.4 GHz ISM band OOK transceiver with high energy efficiency for biomedical implantable applications," *IEEE Transactions on Biomedical Circuits and Systems*, vol. 14, no. 1, pp. 113–124, 2020.

[6] B. Chatterjee, A. Srivastava, D. H. Seo, D. Yang, and S. Sen, "A context-aware reconfigurable transmitter with 2.24 pj/bit, 802.15.6 NB-HBC and 4.93 pj/bit, 400.9 MHz medradio modes with 33.6% transmit efficiency," in *IEEE Radio Frequency Integrated Circ. Symposium*, 2020, pp. 75–78.

[7] H. Rahmani and A. Babakhani, "A 1.6mm^3 wirelessly powered reconfigurable fdd radio with on-chip antennas achieving 4.7 pJ/b TX and 1 pJ/b RX energy efficiencies for medical implants," *2020 IEEE Custom Integrated Circuits Conference (CICC)*, pp. 1–4, 2020.

[8] Z. Safarian and H. Hashemi, "Wideband multi-mode CMOS VCO design using coupled inductors," *IEEE Transactions on Circuits and Systems I: Regular Papers*, vol. 56, no. 8, pp. 1830–1843, 2009.